Retrieving local effective constitutive parameters for anisotropic photonic crystals

C. Tserkezis and N. Stefanou
Section of Solid State Physics, University of Athens, Panepistimioupolis, GR-157 84 Athens, Greece
(Received 27 November 2009; revised manuscript received 13 January 2010; published 5 March 2010)

We propose a method for calculating average local effective permittivity and permeability tensors for anisotropic photonic crystals through least-squares fits of sets of data points, obtained by rigorous, systematic complex-band-structure, and reflection calculations for all propagation directions, to appropriate analytic expressions. The proposed methodology is applied on a specific example of a tetragonal structure of metallic nanoshells, which is a uniaxial photonic crystal of resonant units. Our results demonstrate the efficiency of the method at low and moderate frequencies and, at the same time, reveal the inability to define local effective constitutive parameters in regions of resonance gaps.

DOI: 10.1103/PhysRevB.81.115112 PACS number(s): 42.70.Qs, 42.25.Bs, 73.20.Mf, 78.67.Bf

I. INTRODUCTION

The effective electromagnetic (EM) response of photonic crystals can be described, in general, by permittivity and permeability tensors that depend on the angular frequency ω and the wave vector $\mathbf{q}$.[1] A photonic crystal may consist, for example, of a periodic arrangement of inclusions (scatterers) in an otherwise homogeneous host material.[2,3] If the wavelength of the EM field is much larger than the size of the scatterers and the distance between them, a local effective-medium description through EM parameters that depend, possibly, on the frequency but not on the wave vector may be applicable. In a photonic crystal of cubic symmetry, the three principal axes are physically equivalent. Therefore one expects this crystal to be isotropic in the long-wavelength limit with an optical response described by scalar permittivity and permeability functions, $\varepsilon(\omega)$ and $\mu(\omega)$, respectively. However, this is clearly not the case for photonic crystals of lower symmetry, where tensor, instead of scalar, constitutive parameters are relevant. In recent years, the problem of homogenization of anisotropic photonic crystals has emerged as an important issue, also in relation to optical metamaterials.[4–12]

Owing to their simplicity, quasistatic effective-medium theories such as the Maxwell-Garnett[13] or the Bruggeman[14] theory and extensions of them for moderate frequencies[15] are widely used for the homogenization of photonic crystals. However, though such approximations are sufficiently accurate in a number of problems, there are situations where they fail or cannot be applied. Closed-form expressions for the effective permittivity of photonic crystals in the long-wavelength limit have been derived within the framework of the plane-wave-expansion band-structure-method.[16–18] This approach can handle arbitrary unit-cell geometries and describe optical anisotropy. However, it suffers from the drawbacks of the plane-wave-expansion method, e.g., its relatively slow convergence in the case of structures with high dielectric contrast, while its extension beyond the quasistatic limit is not straightforward. The optical response of an arbitrary periodic array of particles, in the dipole approximation, can be described by a frequency- and wave-vector-dependent effective dipole polarizability tensor,[19] which, in the long-wavelength (quasistatic) limit, leads to a proper generalization of the Clausius-Mossotti equation.[19,20] The retrieval of local constitutive effective parameters for lattices of electric and magnetic dipole particles was also discussed by Simovski and Tretyakov.[21] On the other hand, a general self-consistent homogenization method, which can describe arbitrary nonmagnetic periodic metamaterials through nonlocal constitutive parameters, has been developed by Silveirinha.[22] However, in order to be useful for practical applications, a homogenization procedure should provide tensors of local effective parameters, which are independent of the polarization and propagation direction of the wave,[21] and additional efforts along this direction have been undertaken in recent years.[23–25]

In the present paper we propose a procedure to obtain a full set of local effective parameters that describe the optical response of a three-dimensional (3D), generally anisotropic, photonic crystal, at low and moderate frequencies, by properly averaging over all propagation directions the results of rigorous, full-electrodynamic calculations of the complex photonic band structure and reflection coefficients. By solving exactly the problem of reflection of light by a flat surface of the bulk crystal normal to its optical axis and calculating the corresponding complex photonic band structure, we obtain reliable local effective parameters that can describe the anisotropic optical metamaterial response in any configuration, e.g., curved metamaterial surfaces, composite structures involving this metamaterial, etc., without the need of complicated multiple-scattering calculations. Clearly, this is the first, but very important, step in the process of designing and studying more complex structures and geometries of metamaterials[26] by avoiding cumbersome calculations. In Sec. II we report explicit expressions for the dispersion relations and reflection coefficients of (uniaxially) anisotropic media and describe how these equations can be used to obtain average effective parameters for photonic crystals of the appropriate symmetry. In Sec. III we briefly review the main points of the layer-multiple-scattering method for 3D photonic crystals and discuss in some more detail the appropriate eigenvalue equations for the complex-band-structure and reflection calculations that will be carried out in this work. The applicability of the proposed methodology is demonstrated on a specific example of a tetragonal crystal of metal-coated silica nanospheres in Sec IV. Finally, the last section summarizes the main results of this paper.

II. WAVE PROPAGATION IN ANISOTROPIC MEDIA

The permittivity and permeability of an anisotropic homogeneous material are second-rank tensors.[27] Though our retrieval method can be applied to any kind of anisotropic photonic crystal, in the present work we shall be concerned with uniaxial media with their optical axis along the z direction, in which case the (relative) permittivity and permeability tensors have the forms

$$\boldsymbol{\varepsilon} = \begin{pmatrix} \varepsilon_1 & 0 & 0 \\ 0 & \varepsilon_1 & 0 \\ 0 & 0 & \varepsilon_z \end{pmatrix}, \tag{1}$$

$$\boldsymbol{\mu} = \begin{pmatrix} \mu_1 & 0 & 0 \\ 0 & \mu_1 & 0 \\ 0 & 0 & \mu_z \end{pmatrix} \tag{2}$$

in the (x,y,z) coordinate system. For a plane wave of angular frequency ω and wave vector $\mathbf{q}$ propagating in such a medium the dispersion relations are[28]

$$\frac{q_\parallel^2}{\varepsilon_1 \mu_z} + \frac{q_{(\mathrm{TE})z}^2}{\varepsilon_1 \mu_1} = \frac{\omega^2}{c^2} \tag{3}$$

for transverse electric (TE) polarization, i.e., if the electric field is perpendicular to the optical axis z, and

$$\frac{q_\parallel^2}{\varepsilon_z \mu_1} + \frac{q_{(\mathrm{TM})z}^2}{\varepsilon_1 \mu_1} = \frac{\omega^2}{c^2} \tag{4}$$

for transverse magnetic (TM) polarization, i.e., if the magnetic field is perpendicular to the optical axis z, where c is the velocity of light in vacuum and $\mathbf{q}_\parallel=(q_x,q_y)$. Obviously, if at a given frequency ω we have sets of data points $(\mathbf{q}_\parallel, q_{(\mathrm{TE})z})$ and $(\mathbf{q}_\parallel, q_{(\mathrm{TM})z})$ corresponding to the dispersion relations in Eqs. (3) and (4), we cannot specify by some procedure all four independent EM parameters ε_1, ε_z, μ_1, and μ_z at this frequency. For example, if we recast Eqs. (3) and (4) in the form of linear equations $y=ax+b$, for $q_{(\mathrm{TE})z}$ or $q_{(\mathrm{TM})z}$ versus $q_\parallel^2$, through least-squares fits of the corresponding data one can only obtain the coefficients μ_1/μ_z, $\varepsilon_1\mu_1$, and $\varepsilon_1/\varepsilon_z$; and of course, the goodness (accuracy) of the fits, the irrelevance of the direction of $\mathbf{q}_\parallel$, and the coincidence of the values of $\varepsilon_1\mu_1$ deduced independently from Eqs. (3) and (4) will corroborate the assumption of a uniaxial, local homogeneous medium.

In order to be able to determine all four independent EM parameters, one can consider, in addition, the reflection coefficient of a plane wave incident from a homogeneous and isotropic medium with (relative) permittivity ε_i and permeability μ_i on the uniaxial medium under consideration. Assuming that the interface between the two media is perpendicular to the optical axis of the uniaxial medium, we have[29]

$$r_{(\mathrm{TE})} = \frac{\sqrt{\varepsilon_i\mu_i\omega^2/c^2 - q_\parallel^2} - \mu_i\sqrt{(\varepsilon_1/\mu_1)(\omega^2/c^2) - q_\parallel^2/(\mu_1\mu_z)}}{\sqrt{\varepsilon_i\mu_i\omega^2/c^2 - q_\parallel^2} + \mu_i\sqrt{(\varepsilon_1/\mu_1)(\omega^2/c^2) - q_\parallel^2/(\mu_1\mu_z)}} \tag{5}$$

or

$$r_{(\mathrm{TM})} = \frac{\sqrt{\varepsilon_i\mu_i\omega^2/c^2 - q_\parallel^2} - \varepsilon_i\sqrt{(\mu_1/\varepsilon_1)(\omega^2/c^2) - q_\parallel^2/(\varepsilon_1\varepsilon_z)}}{\sqrt{\varepsilon_i\mu_i\omega^2/c^2 - q_\parallel^2} + \varepsilon_i\sqrt{(\mu_1/\varepsilon_1)(\omega^2/c^2) - q_\parallel^2/(\varepsilon_1\varepsilon_z)}} \tag{6}$$

for TE- or TM-polarized incident waves, respectively. These waves excite modes of the uniaxial medium corresponding to the dispersion relation in Eq. (3) or Eq. (4), respectively, and, therefore, the transmitted and reflected waves maintain the same polarization as the incident wave. From nonlinear least-squares fits of data points $(\mathbf{q}_\parallel, r_{(\mathrm{TE})})$ and $(\mathbf{q}_\parallel, r_{(\mathrm{TM})})$ to Eq. (5) or Eq. (6) one can obtain $\mu_1\mu_z$, ε_1/μ_1, and $\varepsilon_1\varepsilon_z$, considering them as adjustable parameters. Again, the goodness of the fits, the irrelevance of the direction of $\mathbf{q}_\parallel$, and the coincidence of the values of ε_1/μ_1 deduced independently from Eqs. (5) and (6) will corroborate the assumption of a uniaxial, local homogeneous medium. The quantities $\mu_1\mu_z$, ε_1/μ_1, and $\varepsilon_1\varepsilon_z$, deduced from reflection-coefficient data, together with μ_1/μ_z, $\varepsilon_1\mu_1$, and $\varepsilon_1/\varepsilon_z$, deduced from dispersion-relation data can be used to determine the values of all four independent EM parameters at the given frequency through a best-fit procedure. It should be noted that our approach requires fulfillment of a number of equations larger than the number of unknowns. This poses more severe restrictions on the EM parameters and offers a criterion to assess the validity of a local effective-medium description, in contrast to other retrieval procedures, e.g., based only on reflection-coefficient data.[24]

III. LAYER-MULTIPLE-SCATTERING METHOD FOR PHOTONIC CRYSTALS

Rigorous calculations of the complex band structure and reflection coefficients of the photonic crystals that will be considered in the present work will be carried out by the layer-multiple-scattering method.[30–32] This method provides a versatile and efficient computational framework for fast and accurate full-electrodynamic calculations of the optical properties of structures consisting of successive, possibly different, layers of scatterers arranged with the same two-dimensional (2D) periodicity. The properties of the individual scatterers enter only through the corresponding scattering T matrix, which, for homogeneous spherical particles, is given by the closed-form solutions of the Mie scattering problem.[31] For spheres consisting of a number of concentric, homogeneous spherical shells, the T matrix is obtained by an efficient recursive algorithm.[33]

At a first step, in-plane multiple scattering is evaluated in a spherical-wave basis using the single-scattering T matrix and proper propagator functions. Subsequently, interlayer scattering is calculated in a plane-wave basis. Because of the 2D periodicity of the structure in the x-y plane, the component of the wave vector of the incident wave parallel to the layers, $\mathbf{q}_\parallel$, is written as $\mathbf{q}_\parallel=\mathbf{k}_\parallel+\mathbf{g}'$, where $\mathbf{k}_\parallel$, the reduced wave vector in the surface Brillouin zone, is a conserved quantity in the scattering process and $\mathbf{g}'$ is a certain reciprocal vector of the given 2D lattice. Therefore, the wave vector of the incident wave has the form $\mathbf{K}_{\mathbf{g}'}^{\pm}=\mathbf{k}_\parallel+\mathbf{g}' \pm [q^2-(\mathbf{k}_\parallel+\mathbf{g}')^2]^{1/2}\hat{\mathbf{e}}_z$, where $\hat{\mathbf{e}}_z$ is the unit vector

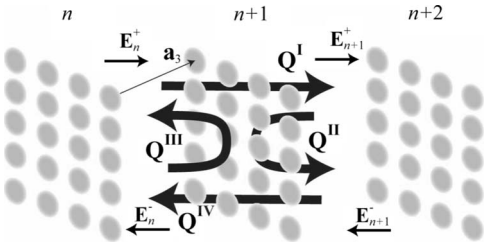

FIG. 1. A photonic crystal built of consecutive layers.

along the z axis, which is taken perpendicular to the layers, and the + or − sign refers to incidence from the left ($z<0$) or from the right ($z>0$), i.e., a wave propagating toward the $z>0$ or the $z<0$ half space, respectively. Since ω and $\mathbf{k}_\parallel$ are conserved quantities in the scattering process, the scattered field will consist of a series of plane waves with wave vectors

$$\mathbf{K}_{\mathbf{g}}^{\pm} = \mathbf{k}_\parallel + \mathbf{g} \pm [q^2 - (\mathbf{k}_\parallel + \mathbf{g})^2]^{1/2}\hat{\mathbf{e}}_z, \quad \forall\, \mathbf{g} \tag{7}$$

and polarizations along $\hat{\mathbf{e}}_1$ and $\hat{\mathbf{e}}_2$ (polar and azimuthal unit vectors, respectively, associated with every $\mathbf{K}_{\mathbf{g}}^s$, $s=\pm$). Though the scattered field consists, in general, of a number of diffracted beams corresponding to different 2D reciprocal-lattice vectors $\mathbf{g}$, only beams for which $K_{\mathbf{g}z}^s$ is real constitute propagating waves. When $(\mathbf{k}_\parallel+\mathbf{g})^2>q^2$ the corresponding wave decays to the right for $s=+$, and to the left for $s=-$; and the corresponding unit vectors $\hat{\mathbf{e}}_{\mathrm{p}}$ become complex but they are still orthonormal ($\hat{\mathbf{e}}_{\mathrm{p}}\cdot\hat{\mathbf{e}}_{\mathrm{p}'}=\delta_{\mathrm{pp}'}, \mathrm{p},\mathrm{p}'=1,2$). The waves transmitted through and reflected from a single layer are obtained by appropriate transmission and reflection matrices: $\mathbf{Q}^{\mathrm{I}}_{\mathbf{gp};\mathbf{g}'\mathrm{p}'}$ and $\mathbf{Q}^{\mathrm{III}}_{\mathbf{gp};\mathbf{g}'\mathrm{p}'}$ for incidence from the left and $\mathbf{Q}^{\mathrm{IV}}_{\mathbf{gp};\mathbf{g}'\mathrm{p}'}$ and $\mathbf{Q}^{\mathrm{II}}_{\mathbf{gp};\mathbf{g}'\mathrm{p}'}$ for incidence from the right, respectively.[31,32] The Q matrices of multilayers with the same 2D periodicity are obtained by combining the corresponding matrices of the component layers so that to describe multiple scattering between the layers to any order. The ratio of the transmitted or reflected energy flux to the energy flux associated with the incident wave defines the transmittance, $\mathcal{T}$, or reflectance, $\mathcal{R}$, respectively, of a given slab.

For a 3D photonic crystal consisting of an infinite periodic sequence of layers, stacked along the z direction, the wave field in the host region between the nth and the $(n+1)$th unit slabs has the form

$$\mathbf{E}(\mathbf{r}) = \sum_{\mathbf{gp}} \{E^+_{\mathbf{gp};n}\exp[i\mathbf{K}^+_{\mathbf{g}}\cdot(\mathbf{r}-\mathbf{A}_n)] + E^-_{\mathbf{gp};n}\exp[i\mathbf{K}^-_{\mathbf{g}}\cdot(\mathbf{r}-\mathbf{A}_n)]\}\hat{\mathbf{e}}_{\mathrm{p}} \tag{8}$$

for given ω and $\mathbf{k}$, where $\mathbf{A}_n$ is an appropriate origin between the nth and the $(n+1)$th slabs. The coefficients $E^s_{\mathbf{gp};n}$ are obviously related to the $E^s_{\mathbf{gp};n+1}$ coefficients through the Q matrices of the unit slab. In matrix form we have (see Fig. 1)

$$\mathbf{E}^+_{n+1} = \mathbf{Q}^{\mathrm{I}}\mathbf{E}^+_n + \mathbf{Q}^{\mathrm{II}}\mathbf{E}^-_{n+1},$$

$$\mathbf{E}^-_n = \mathbf{Q}^{\mathrm{III}}\mathbf{E}^+_n + \mathbf{Q}^{\mathrm{IV}}\mathbf{E}^-_{n+1}. \tag{9}$$

On the other hand, Bloch's theorem implies that

$$\mathbf{E}^s_{n+1} = \exp(i\mathbf{k}\cdot\mathbf{a}_3)\mathbf{E}^s_n, \tag{10}$$

where $\mathbf{a}_3$ is a vector which takes us from a point in the nth slab to an equivalent point in the $(n+1)$th slab and $\mathbf{k}=[\mathbf{k}_\parallel, k_z(\omega,\mathbf{k}_\parallel)]$. For given ω and $\mathbf{k}_\parallel$ one can obtain k_z from the following eigenvalue equation:

$$\begin{pmatrix} \mathbf{Q}^{\mathrm{I}} & \mathbf{Q}^{\mathrm{II}} \\ -[\mathbf{Q}^{\mathrm{IV}}]^{-1}\mathbf{Q}^{\mathrm{III}}\mathbf{Q}^{\mathrm{I}} & [\mathbf{Q}^{\mathrm{IV}}]^{-1}[\mathbf{I}-\mathbf{Q}^{\mathrm{III}}\mathbf{Q}^{\mathrm{II}}] \end{pmatrix}\begin{pmatrix} \mathbf{E}^+_n \\ \mathbf{E}^-_{n+1} \end{pmatrix} = \exp(i\mathbf{k}\cdot\mathbf{a}_3)\begin{pmatrix} \mathbf{E}^+_n \\ \mathbf{E}^-_{n+1} \end{pmatrix}, \tag{11}$$

which follows directly from Eqs. (9) and (10). Alternatively, Eqs. (9) and (10) lead to an eigenvalue equation for the transfer matrix

$$\begin{pmatrix} \mathbf{Q}^{\mathrm{I}}-\mathbf{Q}^{\mathrm{II}}[\mathbf{Q}^{\mathrm{IV}}]^{-1}\mathbf{Q}^{\mathrm{III}} & \mathbf{Q}^{\mathrm{II}}[\mathbf{Q}^{\mathrm{IV}}]^{-1} \\ -[\mathbf{Q}^{\mathrm{IV}}]^{-1}\mathbf{Q}^{\mathrm{III}} & [\mathbf{Q}^{\mathrm{IV}}]^{-1} \end{pmatrix}\begin{pmatrix} \mathbf{E}^+_n \\ \mathbf{E}^-_n \end{pmatrix} = \exp(i\mathbf{k}\cdot\mathbf{a}_3)\begin{pmatrix} \mathbf{E}^+_n \\ \mathbf{E}^-_n \end{pmatrix}. \tag{12}$$

The solutions $k_z(\omega,\mathbf{k}_\parallel)$ resulting from Eq. (11), or equivalently Eq. (12), looked upon as functions of real ω, define, for each $\mathbf{k}_\parallel$, lines in the complex k_z plane. These are termed real-frequency lines and, taken together, constitute the complex band structure of the infinite crystal associated with the given crystallographic plane. A line of given $\mathbf{k}_\parallel$ may be real (in the sense that k_z is real) over certain frequency regions, and be complex (in the sense that k_z is complex) for ω outside these regions. It turns out that for given $\mathbf{k}_\parallel$ and ω, out of the solutions $k_z(\omega,\mathbf{k}_\parallel)$, none or, at best, a few are real and the corresponding eigenvectors represent propagating modes of the EM field in the given infinite crystal. The remaining solutions $k_z(\omega,\mathbf{k}_\parallel)$ are complex and the corresponding eigenvectors represent evanescent waves. These have an amplitude which increases exponentially in the positive or negative z direction and, unlike the propagating waves, do not exist as physical entities in the infinite crystal. However, they are an essential part of the physical solutions of the EM field in the case of a surface or a slab of finite thickness. A region of frequency where propagating waves do not exist, for given $\mathbf{k}_\parallel$, constitutes a frequency gap of the EM field for the given $\mathbf{k}_\parallel$. If over a frequency region no propagating wave exists whatever the value of $\mathbf{k}_\parallel$, then this region constitutes an absolute frequency gap.

The reflection matrix of the corresponding semi-infinite crystal, $\mathbf{R}_\infty$, for given ω and $\mathbf{k}_\parallel$, can be obtained from the set of eigenvectors $\mathbf{f}$ of the transfer matrix on the left-hand side of Eq. (12) as follows. The Bloch eigenmodes are first classified as forward or backward, depending on if they propagate (or decay) along the positive or negative z direction, respectively. This classification for the evanescent modes is straightforward, according to the sign of $\mathrm{Im}\, k_z$. For the propagating modes ($\mathrm{Im}\, k_z=0$), we examine the direction of energy flow, which is determined from the sign of the quantity

$$\mathcal{E}_F = \sum_{\substack{\mathbf{gp} \\ (\mathbf{k}_\parallel + \mathbf{g})^2 < q^2}} (|f^+_{\mathbf{gp}}|^2 - |f^-_{\mathbf{gp}}|^2) - 2\,\mathrm{Im} \sum_{\substack{\mathbf{gp} \\ (\mathbf{k}_\parallel + \mathbf{g})^2 > q^2}} f^+_{\mathbf{gp}} [f^-_{\mathbf{gp}}]^*, \tag{13}$$

where $f^s_{\mathbf{gp}}$ are the components of a given eigenvector.[34] In the numerical implementation of the method we keep a finite number, $g_{\max}$, of reciprocal-lattice vectors (those of the smallest magnitude), in which case we obtain $4g_{\max}$ eigenvalues and corresponding eigenvectors [see Eq. (12)]. Half of them correspond to forward modes and the other half correspond to backward modes, as a result of time-reversal symmetry. Let us now define the $4g_{\max} \times 4g_{\max}$ eigenvector matrix, $\mathbf{F}$, as follows. Its first $2g_{\max}$ columns comprise the eigenvectors corresponding to the forward (+) modes and its last $2g_{\max}$ columns comprise the eigenvectors corresponding to the backward (–) modes. This matrix has a simple physical interpretation. It projects the space of forward and backward Bloch eigenmodes, $\mathbf{V}^+$ and $\mathbf{V}^-$, onto the original plane-wave basis, i.e.,

$$\begin{pmatrix} \mathbf{E}^+_0 \\ \mathbf{E}^-_0 \end{pmatrix} = \begin{pmatrix} \mathbf{F}^{++} & \mathbf{F}^{+-} \\ \mathbf{F}^{-+} & \mathbf{F}^{--} \end{pmatrix} \begin{pmatrix} \mathbf{V}^+ \\ \mathbf{V}^- \end{pmatrix}. \tag{14}$$

By definition, each eigenmode propagates through the crystal without changing its state and, on the other hand, for a semi-infinite crystal, there is no rear surface to reflect the forward into the backward Bloch waves. Therefore, the appropriate boundary condition for the scattering problem of an EM wave incident on a semi-infinite photonic crystal from the homogeneous host material that (it is assumed) extends to infinity is $\mathbf{V}^- = \mathbf{0}$.[35] This condition, applied to Eq. (14), leads to

$$\mathbf{E}^-_0 = \mathbf{F}^{-+}[\mathbf{F}^{++}]^{-1}\mathbf{E}^+_0 \equiv \mathbf{R}_\infty \mathbf{E}^+_0, \tag{15}$$

which defines the reflection matrix, $\mathbf{R}_\infty$, of the semi-infinite photonic crystal.

IV. A TETRAGONAL CRYSTAL OF METALLIC NANOSHELLS

We shall apply our homogenization procedure on a generic anisotropic photonic crystal, namely, a simple tetragonal lattice of silica nanospheres ($\varepsilon_{\text{silica}}=2.13$, $\mu_{\text{silica}}=1$) of radius R_1, coated with a thin concentric metallic shell of thickness D, shown in Fig. 2. We assume that the metallic material is described by the simple, yet effective, Drude relative permittivity[36]

$$\varepsilon_m = 1 - \frac{\omega_p}{\omega(\omega + i\tau^{-1})}, \tag{16}$$

where ω_p is the bulk plasma frequency and τ the relaxation time of the conduction-band electrons that accounts for dissipative losses, and $\mu_m=1$. For convenience, we shall use ω_p as the frequency unit and c/ω_p as the length unit (considering a typical value of 10 eV for $\hbar\omega_p$, c/ω_p corresponds to about 20 nm). These metallic nanoshells are chosen because they are easily tunable resonant units. Plasmons of the outer and inner surfaces of the shell interact with each other and give rise to coupled resonant modes, one below the lower (particlelike) and one above the higher (cavitylike) plasmon modes.[37,38] The interaction and the resulting level shifts increase as the overlap between the corresponding wave fields becomes larger, i.e., by reducing the shell thickness and is more pronounced for the fundamental dipole modes because of their relatively larger spatial extent.[39] Taking $R_1=0.7c/\omega_p$ and $D=0.3c/\omega_p$, the lowest (dipole) plasmon modes of the nanoshells in the given crystalline arrangement create flat resonance bands at moderate frequencies where we shall apply our homogenization procedure, thus making the situation more interesting.[40]

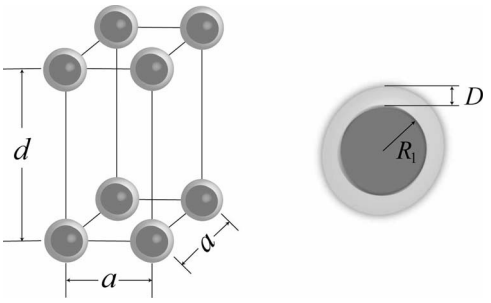

FIG. 2. A schematic view of the primitive cell (left) of the photonic crystal under consideration. A simple tetragonal crystal with lattice constants $a=3c/\omega_p$ and $d=6c/\omega_p$ of nanospheres (right) consisting of a silica core of radius $R_1=0.7c/\omega_p$ and a metallic shell of thickness $D=0.3c/\omega_p$ in air.

The unit cell of the crystal under consideration is shown in Fig. 2. We view the crystal as a sequence of successive square lattices (lattice constant $a=3c/\omega_p$) of nanoshells, stacked along the z direction. The distance between consecutive planes is $d=6c/\omega_p$. Complex photonic band diagrams of this crystal, as calculated by the layer-multiple-scattering method, are displayed in the left-hand panel of Fig. 3. We have deliberately disregarded absorption in the metallic material, taking $\tau^{-1}=0$ in Eq. (16); however, the on-shell layer-multiple-scattering method can also take into account the

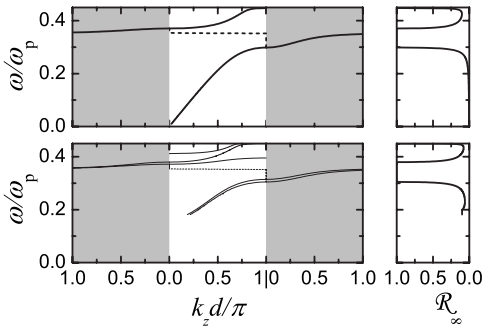

FIG. 3. Left-hand panel: the complex photonic band structure of the crystal shown in Fig. 2 for $\mathbf{k}_\parallel=\mathbf{0}$ (upper diagram) and $\mathbf{k}_\parallel=(0.08,0.04)2\pi/a$ (lower diagram). The thick and thin lines denote doubly degenerate and nondegenerate bands, respectively. Over the gap regions we display the complex bands with the smallest in magnitude imaginary part; their real part is shown by dashed lines and their imaginary part is shown in the gray-shaded areas. Right-hand panel: the corresponding reflection spectra of the semi-infinite crystal.

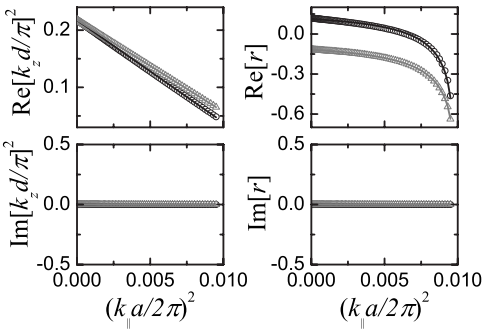

FIG. 4. Fits (solid lines) of dispersion-relation (left-hand panel) and reflection-coefficient (right-hand panel) data (open symbols), obtained from rigorous layer-multiple-scattering calculations for the photonic crystal shown in Fig. 2 at $\omega=0.2\omega_p$, to Eqs. (3), (4) and (5), (6), respectively. Open triangles and circles refer to TE and TM polarizations, respectively.

effect of dissipative losses. In order to ensure adequate convergence in our calculations, we truncate the spherical-wave expansions at $l_{max}=5$ and take into account 25 2D reciprocal lattice vectors. The fact that the (001) surface of the given crystal is a plane of mirror symmetry implies that the frequency bands appear in pairs: $k_z(\omega,\mathbf{k}_\parallel)$ and $-k_z(\omega,\mathbf{k}_\parallel)$; this is why in Fig. 3 we show the bands only for positive k_z. For $\mathbf{k}_\parallel=\mathbf{0}$, i.e., along the [001] direction, the bands have the symmetry of the irreducible representations of the C_{4v} point group: Δ_1, Δ_2, $\Delta_{1'}$, and $\Delta_{2'}$, which are one dimensional, and Δ_5, which is two dimensional.[41] The bands shown in the top-left diagram of Fig. 3 are all doubly degenerate; they have the Δ_5 symmetry. Along another direction in the Brillouin zone, which is invariant under the symmetry operations of a (smaller) point group that does not possess a two-dimensional irreducible representation, all bands are nondegenerate (see bottom-left diagram of Fig. 3). This splitting of the doubly degenerate bands should be accounted for by a proper anisotropic effective medium, according to Eqs. (3) and (4). It is worth noting that, in the strict sense, such a splitting occurs even in a cubic crystal. However, in this case, our calculations show that the anisotropy is negligibly small, in agreement with the assumption of an optically isotropic effective medium, at low and moderate frequencies.

The dispersion diagrams of the photonic crystal under consideration in the frequency region of interest are characterized by broad bands of extended states and narrow bands of localized states that originate from the dipole particlelike plasmon modes of the individual nanoshells, weakly interacting between them. Anticrossing interaction between these bands leads to the opening of frequency gaps. In the gap regions there are no propagating modes of the EM field and the real-frequency dispersion lines continue analytically in the complex k_z plane.[42] There is, in principle, an infinite number of such complex bands but, over a gap region, it is the complex band of the appropriate symmetry with the smallest in magnitude imaginary part of k_z, which determines the decay of EM waves along the given direction. Obviously, the corresponding reflectivity of the semi-infinite crystal equals unity in the gap regions, as shown in the right-hand panel of Fig. 3.

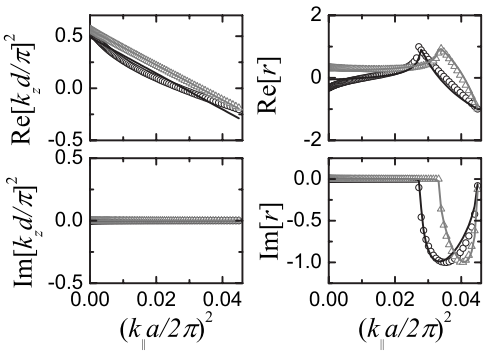

FIG. 5. The same as Fig. 4, at $\omega=0.43\omega_p$.

We have carried out systematic band-structure and reflection calculations along many directions corresponding to different points $\mathbf{q}_\parallel(=\mathbf{k}_\parallel)$ for the given photonic crystal in the frequency region under consideration. The results obtained must follow Eqs. (3), (4) and (5), (6), respectively, and they indeed do so outside the gap region as shown in Figs. 4 and 5. From the corresponding fits we setup a system of eight equations for the four unknown parameters, ε_1, ε_z, μ_1, and μ_z, which is subsequently solved by a second (nonlinear) least-squares fit procedure. We adopt as a quantitative estimate of the goodness of the fits at a given frequency the corresponding average standard deviation. The variation in the effective constitutive parameters versus frequency, obtained in the above manner, is displayed in Fig. 6 together with the corresponding standard deviation. It can be seen that, with the exception of the region of resonance gaps where local constitutive parameters are physically meaningless[21] and our fitting procedures fail completely, average effective permittivity and permeability tensors can be defined with sufficient accuracy. The anisotropy of the permittivity, $\varepsilon_1-\varepsilon_z$, grows from 0.07 at low frequencies to very large values on the order of 100 as we approach the gap and decreases again above the gap, while $\mu_1-\mu_z$ is less than 0.02 over the whole frequency range under consideration.

Our homogenization procedure defines a complete set of local effective parameters based on the idea that a hypothetical homogeneous, anisotropic material mimics the response

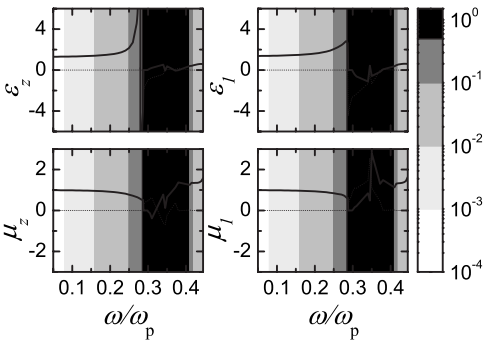

FIG. 6. Average effective constitutive parameters (their real and imaginary parts are shown by solid and dotted lines, respectively) of the photonic crystal shown in Fig. 2. The standard deviation in the fitting procedure at different frequencies is shown by gray-shaded areas. In black regions, average effective parameters are meaningless.

of the photonic crystal, in the sense that light propagation along any direction in the two media obeys the same dispersion relations and, also, an externally incident wave, impinging at any angle on their surface, produces the same reflected field in the far zone. We note that the effective parameters do not describe the exact form of the wave field inside the actual crystal where, at a given frequency, it has the form of a Bloch wave and not a simple plane wave. It should also be pointed out that, as for any effective-medium approximation, in order for our homogenization procedure to be physically meaningful, there must be a single dominant relevant Bloch mode at a given frequency. Moreover, the wavelength in the embedding medium must be larger than the in-plane period of the structure, so that there is only a single propagating mode of the reflected field, for $\mathbf{g}=\mathbf{0}$ [see Eq. (7)]. All other components of the wave field, corresponding to higher-order diffracted beams, are evanescent.

V. CONCLUSION

In summary, we presented a general procedure to evaluate average local effective parameters of anisotropic photonic crystals, by fitting the results of systematic, rigorous complex-band-structure and reflection-coefficient calculations, over a wide range of propagation directions, to appropriate analytic expressions. The quality of these fits provides an additional means to control the validity of a local effective-medium description of the composite structure in different spectral regions. We applied the proposed approach on a specific example of a tetragonal crystal of metallic nanoshells using the full-electrodynamic on-shell layer-multiple-scattering method, which allows one to calculate, also, the complex propagation constants in gap regions and/or describe lossy photonic crystals. Our results show that the optical response of the given structure, along any direction, can be described with sufficient accuracy by permittivity and permeability tensors that correspond to a local, homogeneous uniaxial effective medium. This description is valid at low and moderate frequencies, except in spectral regions of resonance gaps.

ACKNOWLEDGMENT

This work was supported by the research program "Kapodistrias"of the University of Athens.

[1] A. L. Efros, Phys. Rev. E **70**, 048602 (2004).
[2] J. D. Joannopoulos, R. D. Meade, and J. N. Winn, *Photonic Crystals: Molding the Flow of Light* (Princeton University Press, New York, 1995).
[3] K. Sakoda, *Optical Properties of Photonic Crystals* (Springer-Verlag, Berlin, 2001).
[4] I. V. Lindell, S. A. Tretyakov, K. I. Nikoskinen, and S. Ilvonen, Microwave Opt. Technol. Lett. **31**, 129 (2001).
[5] L. Hu and S. T. Chui, Phys. Rev. B **66**, 085108 (2002).
[6] D. R. Smith and D. Schurig, Phys. Rev. Lett. **90**, 077405 (2003).
[7] L. Zhou, C. T. Chan, and P. Sheng, Phys. Rev. B **68**, 115424 (2003).
[8] X. L. Chen, M. He, Y. X. Du, W. Y. Wang, and D. F. Zhang, Phys. Rev. B **72**, 113111 (2005).
[9] N.-H. Shen, Q. Wang, J. Chen, Y.-X. Fan, J. Ding, H.-T. Wang, Y. Tian, and N.-B. Ming, Phys. Rev. B **72**, 153104 (2005).
[10] J. Schilling, Phys. Rev. E **74**, 046618 (2006).
[11] W. T. Lu and S. Sridhar, Phys. Rev. B **77**, 233101 (2008).
[12] N.-H. Shen, S. Foteinopoulou, M. Kafesaki, T. Koschny, E. Ozbay, E. N. Economou, and C. M. Soukoulis, Phys. Rev. B **80**, 115123 (2009).
[13] J. C. Maxwell-Garnett, Philos. Trans. R. Soc. London, Ser. A **203**, 385 (1904).
[14] D. A. G. Bruggeman, Ann. Phys. **24**, 636 (1935).
[15] R. Ruppin, Opt. Commun. **182**, 273 (2000).
[16] R. Tao, Z. Chen, and P. Sheng, Phys. Rev. B **41**, 2417 (1990).
[17] S. Datta, C. T. Chan, K. M. Ho, and C. M. Soukoulis, Phys. Rev. B **48**, 14936 (1993).
[18] A. A. Krokhin, P. Halevi, and J. Arriaga, Phys. Rev. B **65**, 115208 (2002).
[19] B. N. J. Persson and A. Liebsch, Phys. Rev. B **28**, 4247 (1983).
[20] C. K. Lo, J. T. K. Wan, and K. W. Yu, J. Phys.: Condens. Matter **13**, 1315 (2001).
[21] C. R. Simovski and S. A. Tretyakov, Phys. Rev. B **75**, 195111 (2007).
[22] M. G. Silveirinha, Phys. Rev. B **75**, 115104 (2007).
[23] S. Riikonen, I. Romero, and F. J. García de Abajo, Phys. Rev. B **71**, 235104 (2005).
[24] I. Romero and F. J. García de Abajo, Opt. Express **17**, 22012 (2009).
[25] G. P. Ortiz, B. E. Martínez-Zérega, B. S. Mendoza, and W. L. Mochán, Phys. Rev. B **79**, 245132 (2009).
[26] C. Rockstuhl, F. Lederer, C. Etrich, T. Pertsch, and T. Scharf, Phys. Rev. Lett. **99**, 017401 (2007).
[27] L. D. Landau and E. M. Lifshitz, *Electrodynamics of Continuous Media* (Pergamon, New York, 1960).
[28] J. Brandmüller, A. Lehmeyer, K. M. Häussler, and L. Merten, Phys. Status Solidi B **117**, 323 (1983).
[29] A. Lehmeyer, L. Merten, and K. M. Häussler, Phys. Status Solidi B **118**, 675 (1983).
[30] N. Stefanou and A. Modinos, J. Phys.: Condens. Matter **3**, 8135 (1991).
[31] N. Stefanou, V. Yannopapas, and A. Modinos, Comput. Phys. Commun. **113**, 49 (1998).
[32] N. Stefanou, V. Yannopapas, and A. Modinos, Comput. Phys. Commun. **132**, 189 (2000).
[33] N. Stefanou, C. Tserkezis, and G. Gantzounis, Proc. SPIE **6989**, 698910 (2008).
[34] L. C. Botten, N. A. Nicorovici, R. C. McPhedran, C. Martijn de Sterke, and A. A. Asatryan, Phys. Rev. E **64**, 046603 (2001).
[35] Z.-Y. Li and K.-M. Ho, Phys. Rev. B **68**, 155101 (2003).
[36] N. W. Ashcroft and N. D. Mermin, *Solid State Physics* (Saunders, New York, 1976).
[37] E. Prodan, C. Radloff, N. J. Halas, and P. Nordlander, Science

302, 419 (2003).
[38] T. V. Teperik, V. V. Popov, and F. J. García de Abajo, Phys. Rev. B **69**, 155402 (2004).
[39] C. Tserkezis, G. Gantzounis, and N. Stefanou, J. Phys.: Condens. Matter **20**, 075232 (2008).
[40] C. Tserkezis, J. Phys.: Condens. Matter **21**, 155404 (2009).
[41] J. F. Cornwell, *Group Theory in Physics* (Academic, London, 1984), Vol. 1.
[42] G. Gantzounis and N. Stefanou, Phys. Rev. B **72**, 075107 (2005).